JOURNAL OF MATERIALS SCIENCE **38** (2003) 3293–3301

A surface characterisation and microstructural study by Scanning Electron Microscopy of the N-methyl-N-alkylpyrrolidinium tetrafluoroborate organic salts

J. EFTHIMIADIS, M. FORSYTH
School of Physics and Materials Engineering, Monash University, PO Box 69M, Clayton, Victoria, 3800, Australia
E-mail: jim.efthimiadis@spme.monash.edu.au

D. R. MACFARLANE
School of Chemistry, Monash University, PO Box 19C, Clayton, Victoria, 3800, Australia

A microstructural characterisation of the family of N-methyl-N-alkylpyrrolidinium tetrafluoroborate organic salts was carried out by observation of powder surface morphologies with the aim of extending the microstructure-property correlation. Inherent difficulties limiting extensive studies of organic solids by SEM, including volatility under vacuum, charging due to electron beam irradiation, and air-sensitivity were overcome with the use of a Field Emission SEM and cryostage attachment. This technique, providing considerable improvements in image quality at low accelerating voltages, enabled direct observation of complex microstructural features in samples exhibiting high temperature plastic crystalline phases (N,N-dimethylpyrrolidinium tetrafluoroborate [$P_{11}BF_4$]; N-methyl-N-ethylpyrrolidinium tetrafluoroborate [$P_{12}BF_4$]; N-methyl-N-propylpyrrolidinium tetrafluoroborate [$P_{13}BF_4$]). Extensive lattice imperfections including grain boundaries, slip planes and dislocation pits were observed within particles of approximately 200 μm diameter. The N-methyl-N-butylpyrrolidinium tetrafluoroborate ($P_{14}BF_4$) sample in this series revealed columnar single crystals with high aspect ratios. The origin of plastic flow properties is discussed using single crystal and polycrystalline slip observations and a relationship proposed between defect characteristics and transport properties.

1. Introduction

The successful commercial utilisation of solid-state electrolytes in certain applications such as batteries requires detailed consideration of interfacial phenomena in the device due to complications introduced by the mechanical stability and the ability to withstand dimensional changes associated with stresses produced under charge/discharge cycling and vibrations [1–7]. Where liquid flow is absent, interfacial voids may develop with the passing of current through an interface [8]. In the presence of pressure induced plastic flow, dimensional changes could be accommodated and hence it may be possible for suitably doped organic plastic crystals to be ideal battery electrolyte materials [9].

The plastic crystalline state is a mesophase between the low temperature rigid solid and high temperature liquid/melt, and is typically formed following one or more high entropy solid-solid phase transformations. Such crystals comprise long-range positional ordering of the centres of mass of highly orientationally disordered molecules [10]. The rapid molecular reorientations generate high concentrations of lattice defects which lead typically, as their name implies, to plastic mechanical behaviour [11, 12]. High deformation rates inherent to the plastic crystal phase are suggested to be similar in nature to conventional crystalline materials (e.g., the mechanism of creep) [13], as determined for plastic crystal forming dl-camphor, succinonitrile [13], anthracene [14], and adamante [15].

With the application of stress, whether mechanical (plastic deformation) or thermal (quench) [16], resultant plastic deformation corresponds in general to the net motion of dislocations, termed slip, along favourable crystallographic planes [17–20]. The associated dislocation strain field is of the order of a fraction of a micron to a hundred microns [21, 17]. In metals, the dislocation core radius is of the order, $r_c \approx 10$–20 Å [22]. Dislocations are generated during crystal growth [23, 24], plastic deformation [24], or with the coalescence of vacancies which form during solidification [25]. Crystal growth observations of plastic crystal forming camphor have shown the formation of large

dislocations in the low temperature monoclinic form, their function, the relief of strain produced by crystal growth. Strain during growth in the higher temperature plastic phase is relieved by plastic flow, resulting in the splitting of the large dislocations and the creation of smaller dislocations in that phase [26]. Intersecting dislocations may also produce point defects such as vacancies and interstitial sites [19, 21]. Systematic investigations to determine the mechanism and degree of imperfections in plastic crystalline materials have utilised a variety of etchants, with dislocation arrays and emergence pits being observed [12].

In organic crystals, slip systems depend on the degree of covalent and ionic inter- and intra-molecular bonding as well as the short-range stress field of the dislocation core [27]. Conductivity [28], self-diffusion [29], thermal migration and optical properties [30] are also closely related to such crystalline lattice imperfections [10, 12]. Hence, preparatory procedures and subsequent handling are expected to affect the physicochemical properties of organic materials.

The well established and extensive success of materials characterisation by direct microscopic examination of surface and near-surface microstructure and defects with conventional Scanning Electron Microscopy (SEM) has not transcended to organic solids which are often extremely hygroscopic (posing the problem of transfer into the microscope) and inherently sensitive to electron beam irradiation at conventional operating voltages [31, 32]. Organic crystals typically require stabilisation to withstand vacuum conditions in the microscope observation chamber, and are coated with gold to become conductive [33]. An SEM equipped with a high-resolution Field Emission Gun (FEG) can, because of smaller probe size [34] provide high-resolution topographic information at low operating voltages of uncoated samples with minimal specimen damage and charging [35–37]. This allows the examination of the natural sample surface micromorphology and, with a cryo-attachment, the possibility of low temperature observation under high vacuum without specimen compromise due to exposure with air.

SEM characterisation to probe particulate microstructure and investigate lattice imperfections inherent to plastic crystalline materials has been performed on the N-alkyl-N-methylpyrrolidinium tetrafluoroborate system ($P_{1x}BF_4$) (Fig. 1), where P indicates the pyrrolidinium cation, the subscript 1 indicates the N-methyl substituent and x, the carbon number of the N-alkyl substituent [38]. Compounds, $P_{11}BF_4$, $P_{12}BF_4$, $P_{13}BF_4$, and $P_{14}BF_4$ represent the organic materials comprising those pyrrolidinium based cations and a weakly complexing anion, BF_4^- which undergoes multiple solid-state thermal transitions [38]. Micrographs are presented of the natural, uncoated surface of organic salts transferred into the microscope without exposure to air. The work has also been extended into variable temperature SEM analysis and investigation of deformation characteristics with discussion of defects.

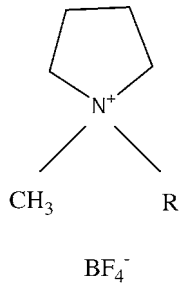

Figure 1 The structure of N-methyl-N-alkylpyrrolidinium tetrafluoroborate organic salts. R = methyl (P_{11}), ethyl (P_{12}), propyl (P_{13}) and butyl (P_{14}).

To our knowledge, this is the first such comprehensive microstructural comparison of an organic crystalline salt system by SEM and is part of an ongoing study of this system [39, 40] and other plastic crystalline and orientationally disordered materials being investigated as potential solid-state electrolytes for secondary battery applications [41].

2. Experimental procedure

2.1. Materials

The synthesis of the N-methyl-N-alkylpyrrolidinium tetrafluoroborate salts involved the metathesis of N-methyl-N-alkylpyrrolidinium iodide with silver tetrafluoroborate, for which detailed preparatory discussion with spectroscopic, physical and electrochemical characterisation is presented elsewhere [38]. Drying involved the use of anhydrous magnesium sulfate, repeated filtering and evaporation with subsequent drying in a vacuum dessicator for several days. Samples were kept in a high-purity nitrogen dry box during storage. The resultant powders were hygroscopic and treated with strict handling under a high purity inert atmosphere.

2.2. Materials characterisation

Powder samples for observation were carefully loaded into specific SEM mountings comprising shallow drilled holes of 5 mm diameter and 3 mm depth. Mounting adhesive was not required to secure powders. Observation of surface morphologies was performed by use of a Philips XL30 FEG SEM. Sample and holder were loaded within a high purity nitrogen atmosphere into an air-tight vacuum attachment and subsequently inserted through a FISONS Instruments Polaron LT7400 cryo-preparation chamber, operating at high vacuum and providing contamination-free surfaces for examination, to the main observation chamber evacuated to $\sim 1 \times 10^{-6}$ mbar. There was no problem of sublimation in the microscope under high vacuum as samples were already dry (as described earlier). Subsequently low temperature work did not suffer from specimen shrinkage or distortion [42].

For secondary electron micrographs, a 2 keV accelerating voltage was used to minimise specimen damage and charging effects. Conventional gold sputtering was not necessary as exemplified by the quality of the micrographs. The use of gold sputtering was avoided due to the thick granular layers of metallisation which typically mask fine structure, particularly at higher magnifications [32, 43].

Variable temperature SEM characterisation was performed with the cryostat attachment utilising liquid nitrogen. A quench was performed initially, then the stage heated against this to regulate temperature. To minimise thermal gradient effects across the sample volume, thermal equilibrium was allowed to be attained by recording micrographs after a 20 min dwell time. The intricacies of low temperature SEM have been discussed in detail elsewhere [42].

3. Results and discussion

3.1. Phase behaviour

On the basis of thermal analysis data (Table I) [38], $P_{11}BF_4$, $P_{12}BF_4$, and $P_{13}BF_4$ are classic plastic crystals all showing high temperature plastic crystalline phases marked by one or more high entropy solid-solid phase transitions at lower temperatures. The compounds have low entropy of fusion (typically less than 20 J/K/mol) [44], a property that is considered characteristic of plastic crystal materials. The plastic state is stable just below the melt and is denoted phase I. Below the solid-solid transition(s) new, more ordered phases (II, III etc.) are formed with decreasing temperature. $P_{14}BF_4$ shows no high temperature transition into the plastic crystalline state and is indicative of "ordinary" crystals with orientational and translational molecular order. Even though micrographs presented are not always in the high temperature plastic crystalline state, $P_{11}BF_4$, $P_{12}BF_4$, and $P_{13}BF_4$ evidently retain their defects to lower temperatures as will be discussed further below.

3.2. Morphology

High-resolution SEM micrographs at ambient temperature of the $P_{1x}BF_4$ system obtained at 2 kV accelerating voltage reveal for $P_{11}BF_4$, $P_{12}BF_4$, and $P_{13}BF_4$, powders with an aspect ratio ∼1:1 on the order of ∼200 μm (100–500 μm) diameter with considerable surface features. In contrast, $P_{14}BF_4$ powders show a definite difference in shape factor, comprised of rod-like or columnar single crystals of ∼1.5 μm cross-sectional diameter, average length ∼6 μms and large aspect ratio of ∼4:1 with almost no surface features. The sharpness of fractured $P_{14}BF_4$ crystallite edges (achieved via physical loading of the sample into SEM mountings) illustrates brittle fracture indicative of non-plastic crystalline behaviour.

For comparison purposes, two related organic salts exhibiting the high temperature plastic crystalline phase, $P_{11}NCF_3SO_2$ and $P_{12}NCF_3SO_2$ show, under the same experimental procedures, powders of 20 μm and 200 μm diameter respectively.

Clearly, the distinction between materials exhibiting high temperature plastic crystalline behaviour ($P_{11}BF_4$-$P_{13}BF_4$) and not ($P_{14}BF_4$) is revealed with SEM in this system. As-grown powders of plastic crystalline materials are spherical with a multitude of lattice imperfections and have proved difficult in single crystal growth. At higher voltages, namely 10 kV, samples were found to be beam sensitive, especially after prolonged irradiation, producing a localised "melting" and irreparable sample damage. No sample compromise occurred as a result of viewing with SEM at 2 kV.

3.3. Lattice defects

Defects in as-grown powders are prominent in the $P_{11}BF_4$, $P_{12}BF_4$ and $P_{13}BF_4$ samples. Fig. 3 shows clearly the periodic grain boundaries which exist in $P_{12}BF_4$. The further visualisation of crystallographic mismatch associated with each neighbouring grain would require an etching process [45].

Direct evidence of lattice mismatch producing a dislocation array is shown in Fig. 4, as obtained at −189°C following a liquid N_2 quench.

The emergence of dislocation ends intersecting the surface as pits within certain grains is related to the crystallographic orientation of slip present in the system which depends on the unit cell characteristics and molecular shape [12]. The appearance of periodic dislocation pits at certain grains only, justifies further that they are not evaporation pits. The density of emergent dislocations corresponds to $10^5/cm^2$ (as determined from Fig. 5) and is consistent with numbers representative of intermediate deformation. Dislocation densities in molecular solids have been shown to vary from small ($<10^5$ cm^{-2}) in the case of crystals grown from the vapour phase, intermediate as grown from solution, to large (10^5–10^7 cm^{-2}) for melt grown crystals [29]. This is expected to have serious consequences in self-diffusion studies in particular [12]. Dislocations in metals arise due to mechanical strain, in the present case their presence can be justified by the fact that deformation has occurred via thermal stress during physical handling and sample loading.

In a single crystal specimen of $P_{13}BF_4$ (Fig. 6) of 10 μm diameter, 50 μm length, macroscopic slip was observed to occur periodically along the most favourable slip plane resulting in the appearance at the surface of steps that loop around the specimen circumference. Similar processes have been shown for metals, e.g., single crystal Zinc [46] in which each step along the length of the crystal is evidence of dislocation movement along the favourable slip system. Dislocation motion usually takes place along the densest packing plane

TABLE I Summary of phase transition temperatures ($T \pm 2$°C)

	T_{VI-V}	T_{V-IV}	T_{IV-III}	T_{III-II}	T_{II-I}	Melting point	ΔS_f (JK^{-1} mol^{-1}) ± 10%
$P_{11}BF_4$	–	−75	−43	61	112	340 (decomp)	–
$P_{12}BF_4$	−68	−55	−41	−29	68	290	5.0
$P_{13}BF_4$	–	–	–	–	45	64	7.0
$P_{14}BF_4$	–	–	–	–	–	142	19

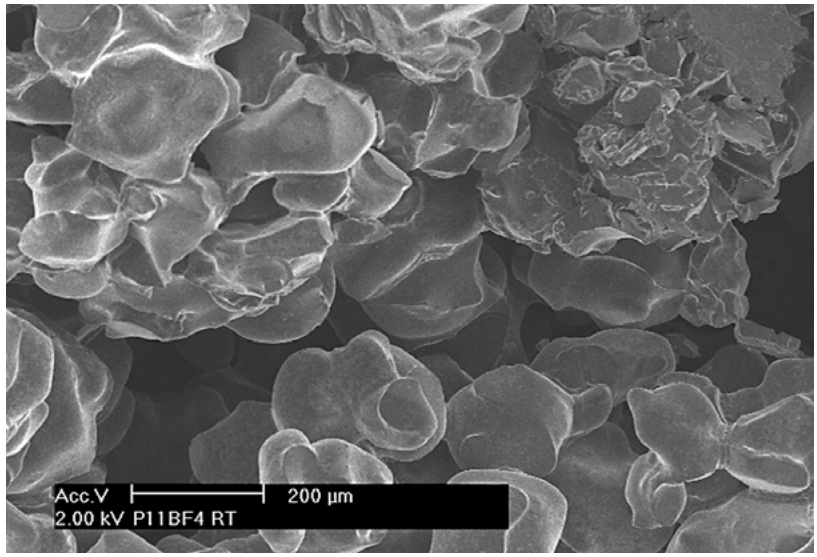

(a)

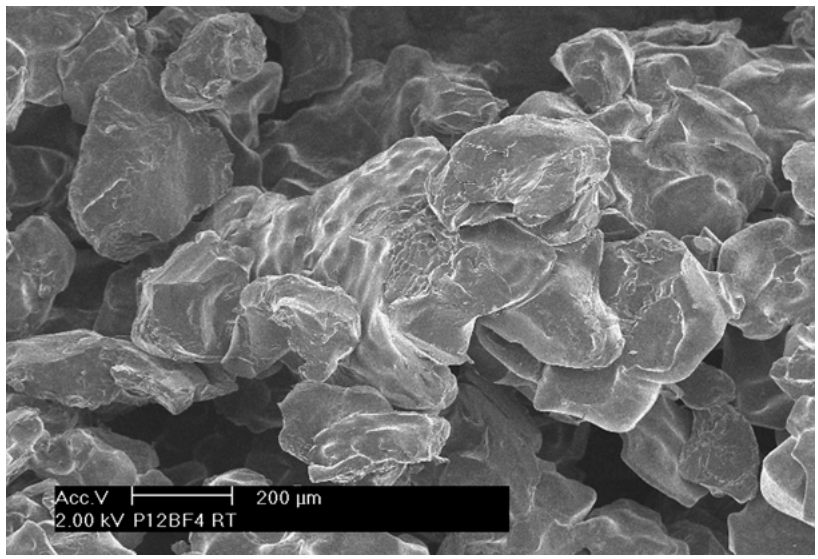

(b)

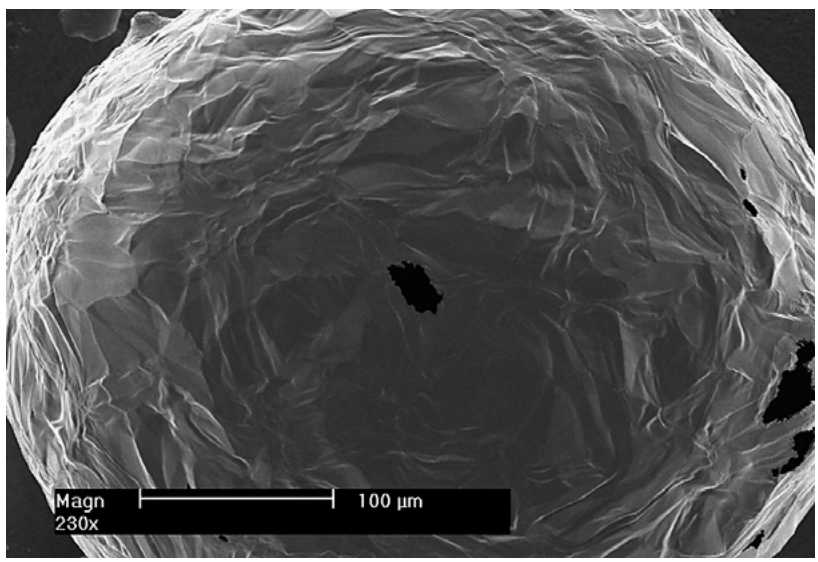

(c)

Figure 2 Ambient temperature FESEM micrographs at 2 kV accelerating voltage of uncoated, as-grown N-alkyl-N-methylpyrrolidinium tetrafluoroborate powders. (a) N,N-dimethylpyrrolidinium tetrafluoroborate ($P_{11}BF_4$) phase III; (b) N-ethyl-N-methylpyrrolidinium tetrafluoroborate ($P_{12}BF_4$) phase II; (c) N-propyl-N-methylpyrrolidinium tetrafluoroborate ($P_{13}BF_4$) phase II; (d) N-butyl-N-methylpyrrolidinium tetrafluoroborate ($P_{14}BF_4$). For comparison purposes, the structural analogues (e) $P_{11}N(CF_3SO_2)_2$; (f) $P_{12}N(CF_3SO_2)_2$. (*Continued*)

(d)

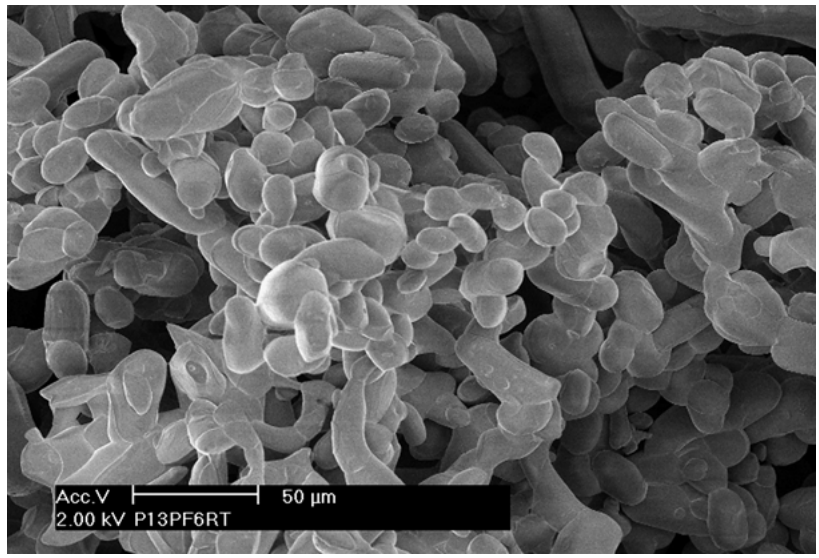

(e)

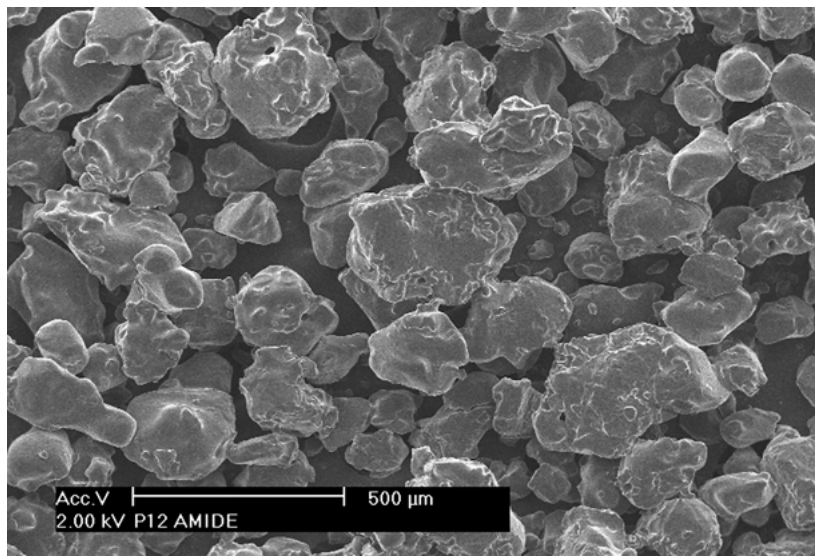

(f)

Figure 2 (*Continued*).

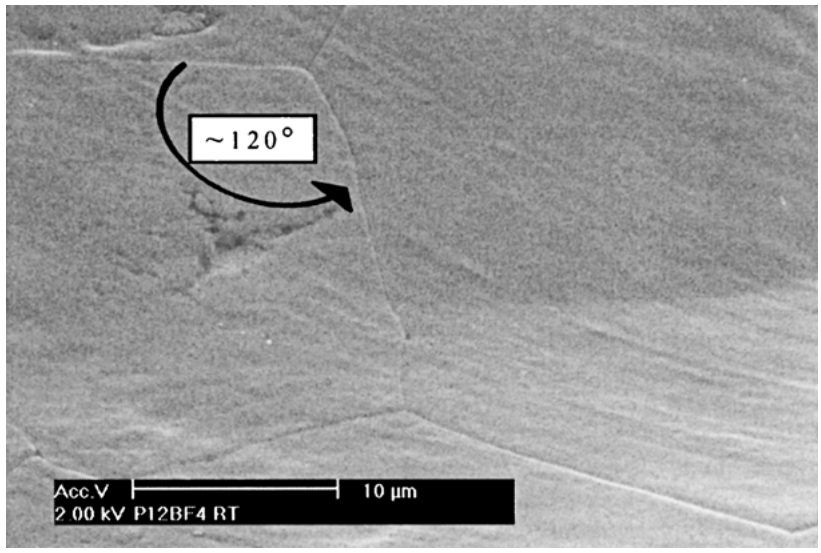

Figure 3 FESEM micrograph of the surface of polycrystalline $P_{12}BF_4$ at ambient temperature in which grain boundaries appear as periodic pentagons.

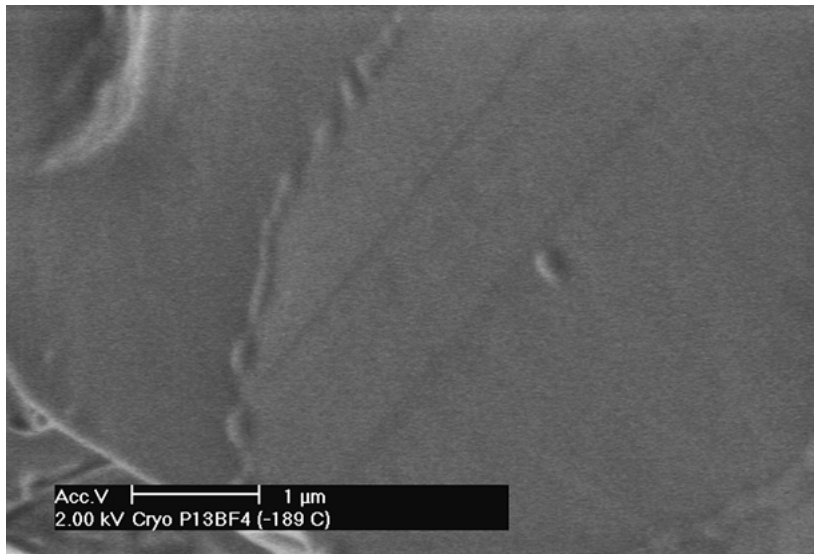

Figure 4 SEM micrograph of the surface of $P_{13}BF_4$ at -189°C showing lattice mismatch between adjacent grains.

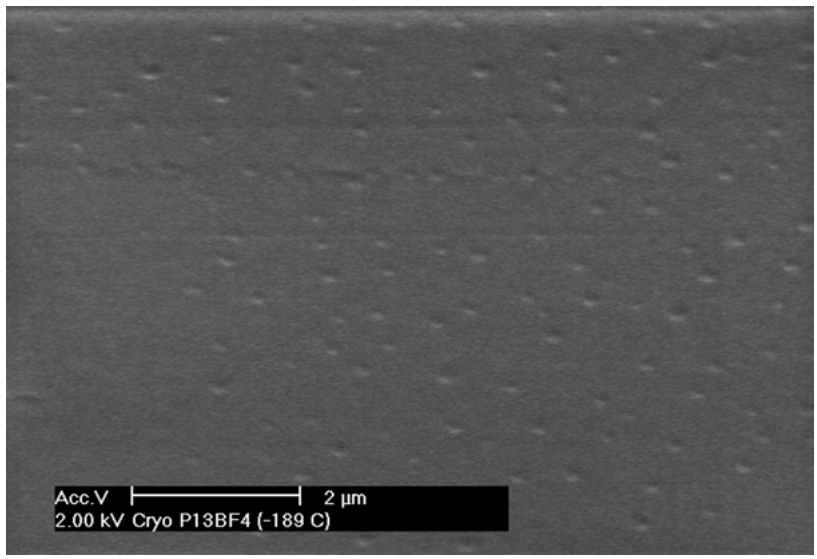

Figure 5 SEM micrograph of the surface of $P_{13}BF_4$ at -189°C showing dislocation pits emerging at the specimen surface.

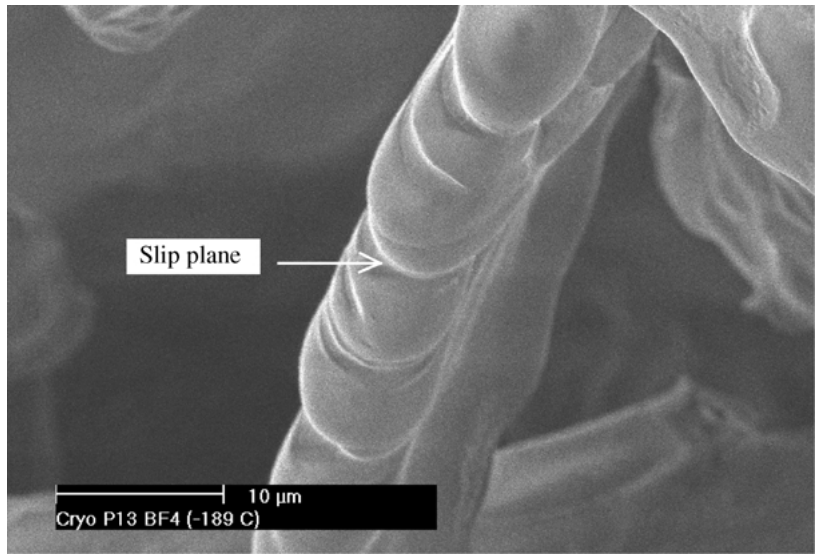

Figure 6 SEM micrograph of single crystal slip planes in $P_{13}BF_4$ at −189°C.

[21], although the limitations of this simplistic argument in molecular crystals have been discussed with respect the organic crystal, tetraoxane [47].

Polycrystalline slip offsets were also shown via direct micrographic example to occur in the $P_{1x}N(CF_3SO_2)_2$ plastic crystal systems within individual grains of a bulk sample. In this case (Fig. 7), slip has occurred along a single slip direction; note that the slip terminates at the grain boundaries which do not lose their coherency.

These micrographs allow the mechanism of vacancy migration and role of grain boundaries to be considered here. The higher interfacial energy of grain boundaries typically cause lattice imperfections (e.g., impurities, vacancies) to preferentially segregate there, acting as sinks (and in some cases even sources) for these defects [48]. The direct microscopic imaging of slip planes (Fig. 6 and [49]) in single and polycrystalline $P_{13}BF_4$ specimens and the structural analogue $P_{12}N(CF_3SO_2)_2$ (Fig. 2f) support the hypothesis that there is a mechanism of vacancy coalescence (thermally or stress activated) to produce dislocations that lead to slip planes occurring within the constraints of the grain boundaries (termed sub-grain). The coalescence of vacancies, particularly in $P_{13}BF_4$ is reinforced by recent positron annihilation lifetime spectroscopy studies which showed an increase in vacancy size with a concomitant decrease in number, as the $P_{13}BF_4$ sample was heated through the phase II to I transition [50]. These ultimately impart on the system its plastic characteristics and this work has suggested dislocations within the grain structure are likely to be responsible. The presence of defect sites which act as paths of rapid diffusion are further supported by Nuclear Magnetic Resonance (NMR) studies in which a composite spectrum, constituting a broad base, superimposed by a sharp narrow peak was observed [39]. On this basis, the diffusion associated with sub-grain dislocations in this system may be of more importance in controlling the observed transport properties such as ionic conductivity than the bulk or grain boundary diffusion. It has been reported previously [51] that the single mechanism of slip in molecular crystals will create steric hindrance between adjacent molecules at the slip boundary. A stabilisation of boundary configuration can only be accomplished by an accompanying rotational displacement about the molecular centre [51]. This may indeed correlate with the proposed rotator phase mechanism for fast ion conduction in many plastic crystals [41, 49, 52–55].

In Fig. 8, we present ionic conductivity data for the plastic crystal forming $P_{11}BF4$ and the non-plastic crystal $P_{14}BF4$. Clearly, the conductivity data for $P_{11}BF_4$

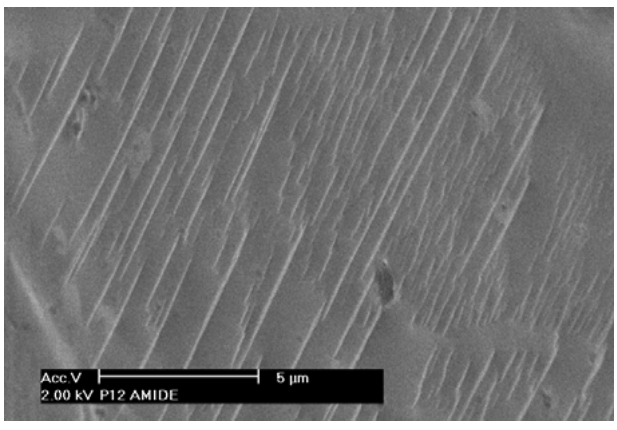

Figure 7 Ambient temperature SEM micrograph of polycrystalline slip occurring in the structural analogue $P_{12}N(CF_3SO_2)_2$.

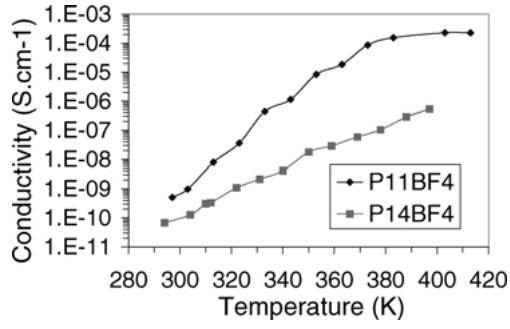

Figure 8 Temperature dependant ionic conductivity in $P_{11}BF_4$ and $P_{14}BF_4$.

is much greater over the entire measured temperature range, hence the interest of plastic crystal forming organic salts as solid-state electrolyte materials.

4. Conclusions

High resolution morphological observations and microstructural characterisation of as-grown N-methyl-N-alkylpyrrolidinium tetrafluoroborate powders by Field Emission SEM with low accelerating voltage and zero exposure to air during transference into the microscope was carried out. A clear distinction in micromorphology was shown to exist between samples in this system exhibiting high temperature plastic crystalline phases ($P_{11}BF_4$, $P_{12}BF_4$, and $P_{13}BF_4$), whilst the non-plastic $P_{14}BF_4$showed columnar crystal morphology. Extensive defects, including dislocations created with the coalescence of vacancies and crystallographic slip in single and polycrystalline specimens, that result in the materials' plastic flow capabilities were directly observed. This type of characterisation confirmed the importance of defects within the system and assisted in correlating microstructure and properties. Furthermore it has shed light in resolving the role of lattice imperfections in the diffusional and transport processes and the phase transformation mechanism inherent to the plastic crystalline nature of this system. As a result of elucidating fundamental structure-property relationships, our aim is the final molecular engineering of related systems with enhancement of desired properties by chemical and structural manipulation [49].

Acknowledgements

The authors would like to thank Stewart Forsyth for preparation of the samples, John Ward and Mark Greaves for assistance with the FESEM. Also we gratefully acknowledge the financial support of the Large ARC Grant 2001: E02003-2404170.

References

1. G. E. BLOMGREN, *J. Power Sources* **81/82** (1999) 112.
2. B. B. OWENS, *ibid.* **90** (2000) 2.
3. T. IWAHORI, I. MITSUISHI, S. SHIRAGA, N. NAKAJIMA, H. MOMOSE, Y. OZAKI, S. TANIGUCHI, H. AWATA, T. ONO and K. TAKEUCHI, *Electrochim. Acta* **45** (2000) 1509.
4. S. SKAARUP, K. WEST, B. ZACHAU-CHRISTIANSEN, M. POPALL, J. KAPPEL, J. KRON, G. EICHINGER and G. SEMRAU, *ibid.* **43** (1998) 1589.
5. M. BALKANSKI, *Solar Energy Mat. Solar Cells* **62** (2000) 21.
6. M. LIU, S. VISCO and L. D. JONGUE, *Electrochim. Acta* **38** (1993) 1289.
7. M. VOINOV, in "Electrode Processes in Solid State Ionics," edited by M. Kleitz and J. Dupuy (D. Reidel Publishing, Dordrecht, 1976) p. 431.
8. C. C. LIANG, in "Proceedings of the NATO Sponsored Advanced Study Institute on Fast Ion Transport in Solids," edited by W. V. Gool (North-Holland Publishing, 1972) p. 19.
9. C. A. ANGELL, *Annual Techn. Report* (U.S. Dept. Energy, Washington, 1986), DOEER45102T1.
10. J. N. SHERWOOD, "The Plastically Crystalline State (Orientationally Disordered Crystals)" (John Wiley & Sons, 1979).
11. *Idem.*, in "The Plastically Crystalline State (Orientationally Disordered Crystals)," edited by J. N. Sherwood (John Wiley & Sons, 1979) p. 39.
12. *Idem.*, *Mol. Cryst. Liq. Cryst.* **9** (1969) 37.
13. G. J. OGILVIE and P. M. ROBINSON, *ibid.* **12** (1971) 379.
14. P. M. ROBINSON and H. G. SCOTT, *ibid.* **11** (1970) 13.
15. B. S. SHAH and J. N. SHERWOOD, *Trans. Farad. Soc.* **67** (1971) 1200.
16. W. D. CALLISTER, "Materials Science and Engineering. An Introduction" (John Wiley & Sons, New York, 1991) p. 158.
17. A. ACHARYA, *J. Mech. Phys. Solids* **49** (2001) 761.
18. L. E. POPOV, S. N. KOLUPAEVA, N. A VIHOR and S. I. PUSPESHEVA, *Comput. Mater. Sci.* **19** (2000) 267.
19. B. S. H. ROYCE, *Disc. Farad. Soc.* **38** (1964) 218.
20. L. M. BROWN, *Mater. Sci. Engin.* A **285** (2000) 35.
21. J. L. BASSANI, A. NEEDLEMAN and E. VAN DER GIESSEN, *Int. J. Solid Struct.* **38** (2001) 833.
22. J. F. JUSTO, V. BULATOV and S. YIP, *Script. Mater.* **36** (1997) 707.
23. H. KLAPPER, *Mater. Chem. and Phys.* **66** (2000) 101.
24. S. AMELINCKX, *Disc. Faraday Soc.* **38** (1964) 7.
25. J. M. THOMAS and J. O. WILLIAMS, *Prog. Solid State Chem.* **6** (1971) 119.
26. J. G. ASTON, in "Physics and Chemistry of the Organic Solid State," edited by D. Fox, M. Labes and A. Weissberger (Interscience, 1963) vol. 1, p. 543.
27. P. J. HALFPENNY, *Condens. Matt.* **1** (1991) 17.
28. J. CORISH and P. W. M. JACOBS, *Surf. Defect Prop. Solids* **2** (1973) 160.
29. J. O. WILLIAMS and J. M. THOMAS, *Trans. Faraday Soc.* **63** (1967) 1720.
30. N. OSTAPENKO, V. I. SUGAKOV and M. T. SHPAK, "Spectroscopy of Defects in Organic Crystals" (Kluwer Academic, Dordrecht, 1993).
31. W. JONES, J. M. THOMAS, J. O. WILLIAMS, M. J. GORRINGE and L. HOBBS, *Mol. Cryst. Liq. Cryst.* **32** (1976) 39.
32. H. JAKSCH, *Mater. World* (1996) 323.
33. C. DEFARGE, O. MALAM ISSA and J. TRICHET, *C.R. Acad. Sci. Paris: Earth and Planet. Sci.* **328** (1999) 591.
34. P. HOVINGTON, R. GAUVIN and D. DROUIN, *Scanning* **19** (1997) 438.
35. T. D. ALLEN, G. R. BENNION, S. A. RUTHERFORD, S. REIPERT, A. RAMAHLO, E. KISELEVA and M. W. GOLDBERG, *ibid.* **19** (1997) 403.
36. S. L. ERLANDSEN, *ibid.* **19** (1997) 323.
37. J. B. PAWLEY, in "Advances in Electronics and Electron Physics," edited by P. W. Hawkes and B. Kazan (Academic Press, New York, 1992) p. 203.
38. S. FORSYTH, J. GOLDING, D. R. MACFARLANE and M. FORSYTH, *Electrochom. Acta* **46** (2001) 1753.
39. J. EFTHIMIADIS, S. J. PAS, M. FORSYTH and D. R. MACFARLANE, *Solid State Ionics* **154-155** (2002) 279.
40. J. EFTHIMIADIS, M. FORSYTH and D. R. MACFARLANE, to be published.
41. D. R MACFARLANE, J. HUANG and M. FORSYTH, *Nature* **402** (1999) 792.
42. D. M. PATERSON, *J. Geol. Soc. (London)* **152** (1995) 131.
43. C. E. JEFFREE and N. D. READ, in "Electron Microscopy of Plant Cells," edited by J. L. Hall and C. Hawes (Academic Press, 1991) p. 313.
44. J. TIMMERMANS, *J. Phys. Chem. Solids* **18** (1961) 1.
45. J. N. SHERWOOD, *Mol. Cryst. Liq. Cryst.* **9** (1969) 37.
46. W. D. CALLISTER, "Materials Science and Engineering. An Introduction" (John Wiley & Sons, New York, 1991) p. 164.
47. T. WATANABE and K. IZUMI, *J. Cryst. Growth* **46** (1979) 747.
48. K. LUCKE and G. GOTTSTEIN, *Acta Metall.* **29** (1981) 779.
49. D. R. MACFARLANE and M. FORSYTH, *Advan. Mater.* **13** (2001) 957.
50. A. J. HILL, P. MEAKIN, J. EFTHIMIADIS, M. FORSYTH and D. R MACFARLANE, to be published.
51. T. KOBAYASHI, Y. FUJIYOSHI and N. UYEDA, *Acta Cryst.* A **38** (1982) 356.
52. D. WILMER, K. FUNKE, M. WITSCHAS, R. BANHATTI, M. JANSEN, G. KORUS, J. FITTER and R. LECHNER, *Physica* B **266** (1999) 60.

53. M. WITSCHAS, H. ECKERT, D. WILMER, R. BANHATTI, K. FUNKE, J. FITTER, R. LECHNER, G. KORUS and M. JANSEN, *Zeit. Physik. Chem.* **214** (2000) 643.
54. K. HORIUCHI, H. TAKAYAMA, S. ISHIMARU and R. IKEDA, *Bull.Chem. Soc. Jpn.* **73** (2000) 307.
55. H. ISHIDA, T. IWACHIDO and R. IKEDA, *Ber. Bunsenges. Phys. Chem.* **96** (1992) 1468.

Received 18 June 2002
and accepted 20 May 2003